Journal of Photonics for Energy

PhotonicsforEnergy.SPIEDigitalLibrary.org

Synthesis and characterization of gold/water nanofluids suitable for thermal applications produced by femtosecond laser radiation

Rosa Mondragón
Rafael Torres-Mendieta
Marco Meucci
Gladys Mínguez-Vega
J. Enrique Juliá
Elisa Sani

SPIE.

Rosa Mondragón, Rafael Torres-Mendieta, Marco Meucci, Gladys Mínguez-Vega, J. Enrique Juliá, Elisa Sani, "Synthesis and characterization of gold/water nanofluids suitable for thermal applications produced by femtosecond laser radiation," *J. Photon. Energy* **6**(3), 034001 (2016), doi: 10.1117/1.JPE.6.034001.

Synthesis and characterization of gold/water nanofluids suitable for thermal applications produced by femtosecond laser radiation

Rosa Mondragón,[a,*] Rafael Torres-Mendieta,[b] Marco Meucci,[c] Gladys Mínguez-Vega,[b] J. Enrique Juliá,[a] and Elisa Sani[c]

[a]Universitat Jaume I, Departamento de Ingeniería Mecánica y Construcción, Avenida de Vicent Sos Baynat, s/n, Castelló de la Plana 12071, Spain

[b]Universitat Jaume I, GROC, Institut de Noves Tecnologies de la Imatge (INIT), Avenida de Vicent Sos Baynat, s/n, Castelló de la Plana 12080, Spain

[c]National Institute of Optics, CNR-INO, Largo Enrico Fermi, 6, Firenze I-50125, Italy

Abstract. A laser-based "green" synthesis of nanoparticles (NPs) was used to manufacture gold NPs in water. The light source is a Ti:Sapphire laser with 30 fs FWHM pulses, 800 nm mean wavelength, and 1 kHz repetition rate. The method involves two stages: (1) pulsed laser ablation in liquids and (2) photo-fragmentation (PF). Highly pure and well-dispersed NPs with a diameter of 18.5 nm that can be stored at room temperature without showing any agglomeration over a period of at least 3 months were produced without the need to use any stabilizer. Transmittance spectra, extinction coefficient, NPs agglomeration dynamics, and thermal conductivity of the nanofluids obtained were analyzed before and after being submitted to thermal cycling and compared to those obtained for commercial gold/water suspensions. Optical properties have also been investigated, showing no substantial differences for thermal applications between NPs produced by the laser ablation and PF technique and commercial NPs. Therefore, nanofluids produced by this technique can be used in thermal applications, which are foreseen for conventional nanofluids, e.g., heat transfer enhancement and solar radiation direct absorption, but offering the opportunity to produce them *in situ* in almost any kind of fluid without the production of any chemical waste. [DOI: 10.1117/1.JPE.6.034001]

Keywords: nanofluid; femtosecond laser; solar radiation; volumetric solar receiver.

Paper 16020 received Feb. 23, 2016; accepted for publication Jun. 28, 2016; published online Jul. 19, 2016.

1 Introduction

In recent years, the use of nanofluids (dilute suspensions with solid particles smaller than 100 nm) has gained attention due to their enhanced properties compared to conventional suspensions containing solids of millimetric or micrometric particle size. The high surface-to-volume ratio and, therefore, large heat transfer interface between particles and fluid, the high dispersion stability with predominant Brownian motion, and reduced particle clogging make nanofluids suitable for different applications.[1] The first widely studied application was the use of colloidal solutions as heat transfer fluids. As early as 1873, Maxwell[2] proposed the addition of small solid particles into a base fluid to increase the thermal conductivity of the suspension. However, the use of millimeter- or micrometer-sized particles led to problems such as poor suspension stability and channel clogging, which limits its practical applicability. To solve these drawbacks, in 1995, Choi[3] proposed the use of nanofluids to increase the thermal conductivity of conventional heat transfer fluids. Since then, many studies and reviews have been published about different properties of nanofluids. Among these physical properties, the properties that

*Address all correspondence to: Rosa Mondragón, E-mail: mondragn@uji.es

1947-7988/2016/$25.00

are usually evaluated are thermal conductivity and heat transfer.[4–8] Different kinds of nanoparticles (NPs) have been investigated for this purpose, including metallic,[9,10] semiconducting[11], and insulating ones,[12] as well as carbon nanostructures and carbon-metal complexes.[13–15]

The first idea for a new concept of solar collector, where the heat transfer fluid itself also acts as a solar absorber, dates back to 1975 and employed India ink.[16] In recent years, due to both the development of nanotechnologies and the growing interest in renewable energies, more particularly, thermal solar energy exploitation, an impressive growth in the number of studies on solar applications of nanofluids has been observed. In particular, the use of a fluid working both as a volumetric light absorber and heat exchanger is advantageous over the classical solution of a transparent fluid exchanging heat with a solid absorber (typically, a black-painted or oxidized surface in close thermal contact with the tubes). Thus, the use of nanofluids as direct solar absorbers in solar collectors has been investigated by several groups[17–20] and with different NPs.[21–25]

It has been demonstrated that the most important factors influencing nanofluid properties are size, shape, and the agglomeration state of NPs.[26,27] These parameters are highly dependent on the production process followed to obtain the nanofluids and on the presence of additives, often needed to disperse NPs. Synthesis of high-purity NPs is very important for any practical application and it is very challenging for the scientific community. In this context, pulsed laser ablation in liquids (PLAL), a technique to create NPs was created in 1987 when, for the first time, Patil et al.[28] reported the laser ablation of a solid iron target in water. Later, using this method, it was discovered that it is possible to obtain NPs. The selection of experimental parameters such as light wavelength, laser fluence, ablation time, repetition rate, or the base fluid itself can modify the shape and size distribution of particles[29] and also its production, with a world record to date of 4 g/h.[30] After the PLAL fabrication phase, the shape and size distribution of particles can be highly modified by a second laser irradiation to promote photo-fragmentation (PF) of NPs in the fluid.[31,32] This second process allows a decrease in the size dispersion and the mean size of the NPs inside the fluid, thereby avoiding the agglomeration phenomenon in the production process. Consequently, by controlling the time of the PF process, it is possible to control the characteristics of the NPs in the nanofluids and their stability.[33] The combination of PLAL and PF techniques (PLAL-PF) promotes the formation of high-purity, well size-controlled, and dispersed NPs inside a liquid without the use of any chemical substance as a stabilizer. Moreover, femtosecond radiation, compared to laser ablation at relatively long time scales (e.g., nanosecond and picosecond), can effectively minimize the laser-plume interaction and reduce the heat affected zones,[34,35] thus obtaining the highest quality and best shape-controlled NPs. Moreover, gold NPs generated by laser ablation in liquids are electron acceptors because of surface atom oxidation,[36,37] which produces a relatively high particle surface charge. The NPs attract oxygen species, and the resulting surface charge triggers electrostatic repulsion providing stable colloids of metallic particles in aqueous media without the need for any stabilizer.

In this work, gold NPs dispersed in water were produced by PLAL-PF and then characterized. The thermal and optical properties of the nanofluids were measured and compared to those of available commercial nanofluids containing additives. The high purity and dispersion of NPs produced by PLAL-PF were checked by means of dynamic light scattering (DLS), transmission electronic microscopy (TEM), and energy dispersive x-ray spectroscopy (EDX) tests. The spectrally resolved optical absorption properties of nanofluids were evaluated and thermal conductivity measurements were carried out by the transient hot wire technique. All samples were submitted to thermal cycles and their properties were evaluated before and after the cycles.

2 Experimental Setup

2.1 *Pulsed Laser Ablation in Liquids–Photo-Fragmentation Experimental Setup*

The typical experimental setup for the PLAL-PF method is shown in Fig. 1. The process consists of two stages. In the first one, the PLAL, a pulsed laser beam is focused on the surface of a target producing ablation, where the ejected material produced by the ablation is captured in a liquid

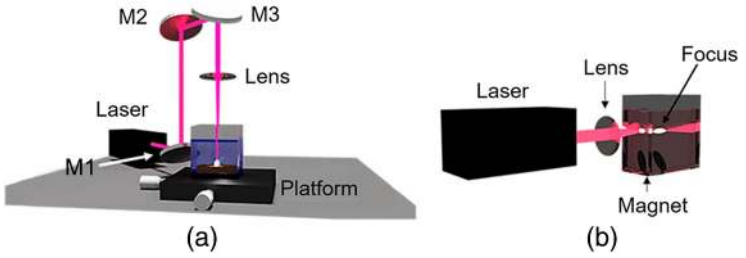

Fig. 1 Experimental setup: (a) arrangement used for PLAL, (b) arrangement used for PLAL-PF.

environment (in this experiment, deionized water 8 MΩ). The interaction between the strong electromagnetic field of the laser radiation and the atoms in the surface of the material promotes the extraction of electrons, thus creating an electronic cloud and leaving a lack of electrons in a localized area on the surface of the target. The ions in the surface are attracted by the electronic cloud through electromagnetic force, thus leaving the bulk material to become NPs with a lack of electrons in the surface. In this step, the ablation process was carried out with a Ti:Sapphire laser (Femtopower Compact Pro, Femto Lasers), with 30 fs FWHM pulses at a wavelength of 800 nm, maximum energy of 1 mJ/pulse, and operating at a repetition rate of 1 kHz. As represented in Fig. 1(a), the laser beam is guided to the sample using a set of mirrors (M1, M2, and M3) that allow the laser radiation to be focused onto the focusing plane of a gold disc (99.99% purity Alfa Aesar) with a diameter of 6.5 mm and a thickness of 2 mm, which is placed at the bottom of a glass cuvette filled with water, using a 75-mm lens, while the beam diameter is 6 mm at the $1/e^2$ point. The cuvette is attached to a two-dimensional motion-controlled stage that is moving at a constant speed of 0.45 mm/s during the experiment, resulting in an ablation duration time of 10.4 min. The thickness of the water layer above the gold disc is about 7 mm while the liquid content in the experimental stage is 1.3 ml, and the peak fluence used to irradiate the sample is 1 Jcm^{-2}. Considering that the optical elements and the liquid itself are going to introduce dispersion, before the optical setup a user-adjustable postcompression stage based on two fused silica Brewster prisms should be used to control the dispersion in the beam delivery path.

The second stage consists of the PF of the particles previously obtained in the first stage. A pulsed laser beam is focused on the nanofluids placed in a quartz cuvette and the energy delivered by the beam in the neighborhood of the focal point of the beam is absorbed by the particles present. The electrons of the atoms on the surface of the particles acquire a lot of energy, which is eventually transmitted to the whole system of particles. The excess of energy promotes the instability of the system and the particle tends to explode, in this way forming smaller particles with a low coalescence rate. PF is carried out by focusing the same pulsed laser beam into the nanofluid thus obtained while constantly stirring it with a magnet to homogenize the process. As depicted in Fig. 1(b), the beam is focused with a 75-mm lens at a depth of 1 cm within the quartz cuvette filled with the nanofluid, the beam diameter being 6 mm, using a peak fluence of 1 Jcm^{-2} under free propagation; however, due to the refraction effects, the value decreases to ∼0.6 Jcm^{-2}. The absorption of high-power radiation generated in the vicinity of the focal point produces the splitting of the biggest particles into smaller particles, thus promoting the production of highly size-controlled and well-dispersed particles.

2.2 *Characterization Techniques and Materials*

The size and shape of primary NPs, as well as the formation of clusters of NPs, were observed by means of transmission electron microscopy using a JEOL 2100 TEM operating at a voltage of 100 kV. To ensure the purity of the gold NPs obtained with the laser-based method, the elemental composition of the NPs was analyzed by means of EDX using an EDX system (Oxford Instruments INCA Penta FETX3) attached to TEM.

The size distributions of NPs in suspension were measured by DLS using a Zetasizer nano ZS (Malvern Instruments Ltd., UK) with a 173 deg scattering angle. Particle size was measured from the velocity of the particles due to their Brownian motion by means of the Einstein–Stokes

Table 1 Investigated samples.

Sample label	
S1	PLAL technique
S2	PLAL technique + thermal cycling
S3	PBS
S4	PBS + thermal cycling
S5	Citrate
S6	Citrate + thermal cycling

equation. The diameter measurement range of the NPs is 0.3 nm to 10 μm with an uncertainty of $\pm 2\%$.

Optical transmittance spectra at room temperature have been measured using a double-beam UV-VIS spectrophotometer (PerkinElmer Lambda900). Nanofluids are held in quartz cuvettes, with a beam path length of 10 mm. The spectral resolution of the measurement was 5 nm. To assess the optical characteristics of both bare Au NPs and Au-NPs aqueous suspensions, transmission spectra were acquired with respect to the base fluid and air reference.

The thermal conductivity of all nanofluids was measured using a KD2 Pro conductimeter (Decagon Devices Inc.). The KD2 Pro is the commercial device that measures thermal conductivity with the help of the transient hot wire technique. In this method, a thin metallic wire is embedded in the test liquid to act as both the heat source and the temperature sensor. The transient hot wire technique works by measuring the temperature/time response of the wire to an abrupt electrical pulse. The sample was introduced in a sealed glass tube (20 mL), where the sensor was inserted vertically. To carry out the test at high temperatures, the tube was immersed in a thermostatic bath with controlled temperature.

Nanofluids produced by the PLAL-PF technique were compared to commercial nanofluids (Sigma Aldrich) containing gold NPs with a 20-nm nominal primary diameter dispersed in water and stabilized in either: (1) 0.1 mM of phosphate buffered saline (PBS) solution or (2) in a citrate buffer solution.

Commercial nanofluids were diluted with distilled water so that the solid content was the same for all samples and equal to the sample obtained by PLAL-PF. The gold concentration was measured by inductively coupled plasma mass spectrometry and was found to be 15 mg/L.

All samples were subjected to heating–cooling cycles to study the influence of the thermal treatment on the properties of NPs and on nanofluid stability. To do this, samples were introduced into a sealed container and heated from room temperature to 100°C in a hot bath. After 1-h heating, nanofluids were allowed to cool down to room temperature. A total of six cycles were run for each sample. Table 1 lists the investigated samples.

3 Results and Discussion

3.1 *Nanoparticles Morphology, Size, and Purity*

To determine the morphology of the gold NPs and the purity of the final solid material, a droplet of nanofluid was dispersed on a carbon-coated copper-based TEM grid. The liquid content was then removed by evaporation so that solid particles could remain on the grid surface, thus facilitating the capture of micrographs. Figure 2 shows TEM micrographs of PLAL-PF and commercial nanofluids, both before and after cycling. From the results, it can be observed that the NPs obtained by the PLAL-PF technique present a higher sphericity than those obtained by chemical processing. In addition, the NPs do not present any changes in terms of morphology or size after the thermal treatment.

Figure 3 shows the EDX patterns that were obtained. In all cases, the presence of copper and carbon has been detected and this is related to the composition of the microscope grid. It can be

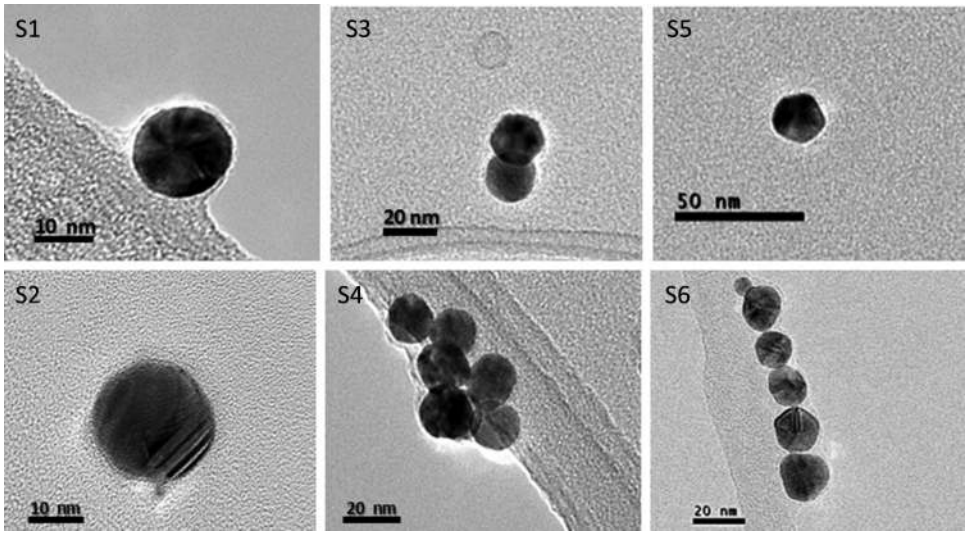

Fig. 2 TEM micrographs of the samples before and after the thermal cycles.

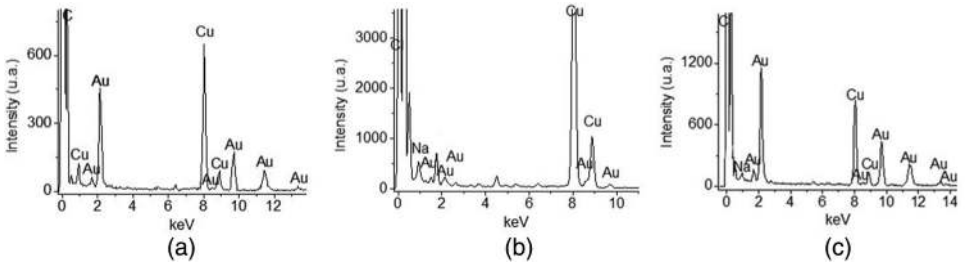

Fig. 3 EDX spectrum of: (a) PLAL-PF produced NPs (S1), (b) commercial NPs in PBS (S3), and (c) commercial NPs in citrate buffer (S5).

observed that, even if gold has been correctly detected in each sample, no other contaminants are present only in the case of PLAL-PF nanofluids. In fact, commercial samples, stabilized with chemicals, also show the elements contained in their dispersants or from the chemical production process itself, such as Na.

The size distributions of NPs suspensions were determined by DLS just after the production of the nanofluid. This technique provides the size distribution of the particles or agglomerates of particles as they are present in the nanofluids in static conditions. Results are shown in Fig. 4. The mean particle size d_{p50} is defined as the size below, of which 50% of particles are comprised, and is very close to the diameter at the peak of the distribution.

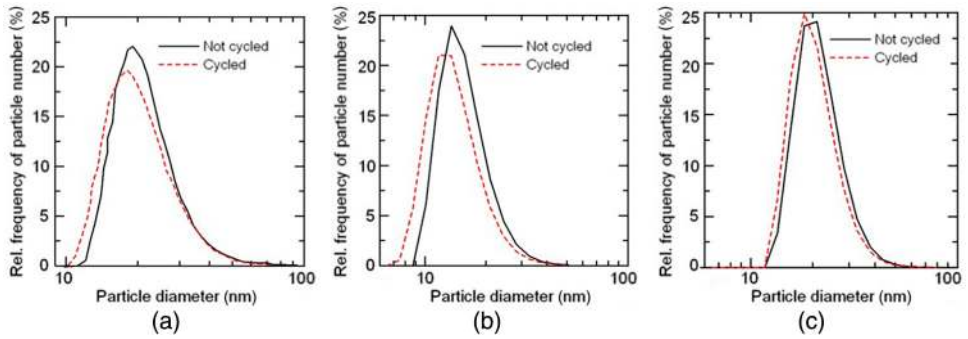

Fig. 4 Particle size distribution: (a) NPs produced by PLAL (S1), (b) commercial NPs in PBS (S3), and (c) commercial NPs in citrate buffer (S5).

Table 2 Mean particle size of nanofluids.

	d_{p50} (nm)	
Sample	Not cycled	Cycled
PLAL-PF	18.5 (S1)	17.4 (S2)
Commercial PBS	15.4 (S1)	14.1 (S4)
Commercial citrate	21.3 (S5)	20.3 (S6)

Results are shown in Table 2. It can be observed that the primary average size of NPs for commercial PBS and citrate buffer nanofluids is 15.4 and 21.3 nm, respectively. In all samples, the NPs are very well dispersed with almost no clustering (clustering is considered to happen when particle sizes larger than $2d_{p50}$ are detected). In all the cases, the NPs distribution is quite narrow, with standard deviation values lower than 5 nm. After thermal treatment, the NPs did not present any noticeable change. A slight reduction in the diameter of the NPs is below the experimental error of the DLS system.

3.2 *Optical Properties*

Figure 5 shows the overall transmittance spectra of the as-prepared samples with respect to air, corrected for the reflectance term. They represent the spectral transmittance of the whole system built with NPs and a base fluid.

It can be appreciated that the spectra show the surface plasmonic peak, corresponding to a minimum in the transmittance spectrum, in a similar spectral position, i.e., at 522.5 ± 2.5 nm, in agreement with the rough similarity of NPs dimensions in the various samples detected by DLS measurements. The difference in the absolute transmittance values of different samples near the plasmonic peak could be due to differences in the molar concentration of different NPs sizes within each polydispersion. In fact, as reported in the literature, both molar concentrations and dimensions of NPs strongly affect optical spectra[38–44] and polydispersed suspensions show an inhomogeneous broadening in the spectra.[40] If the pre- and postcycling spectra (Fig. 6) are compared for each preparation technique, it can be noticed that PLAL and PBS samples show practically no changes; while for citrate samples (S5–S6), the postcycling transmittance is slightly decreased, probably because of some degradation of the citrate additive.

To decouple the contribution to light extinction due to NPs and base fluid, the transmission spectra were acquired using a cuvette filled with distilled water as a reference. Figure 7 shows the

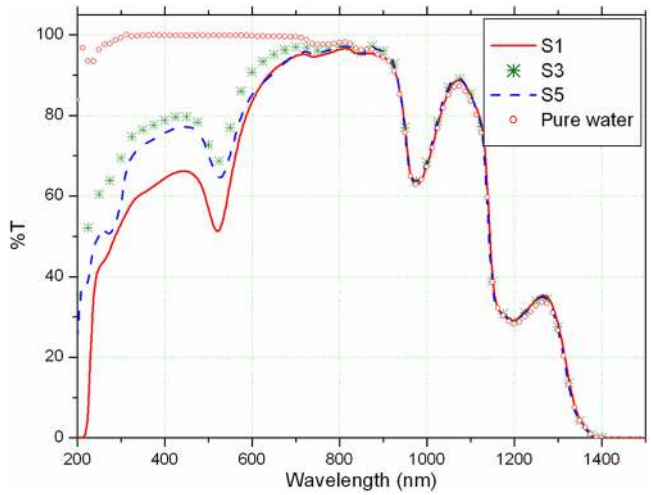

Fig. 5 Transmittance spectra of as-produced samples. The spectrum of pure water is also shown for reference (red dots).

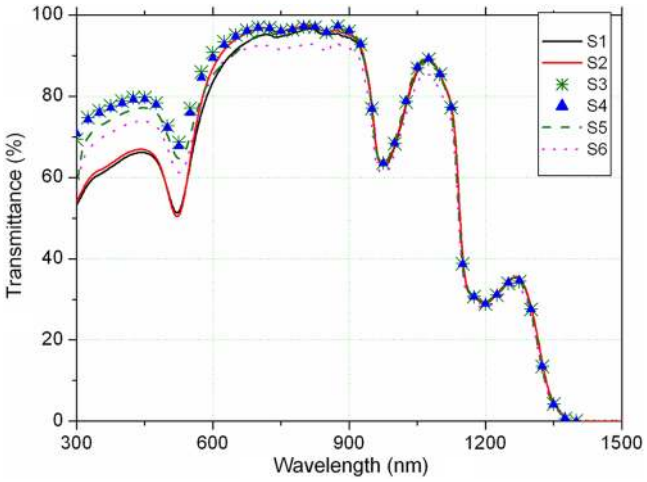

Fig. 6 Comparison of transmittance spectra of as-produced and cycled samples.

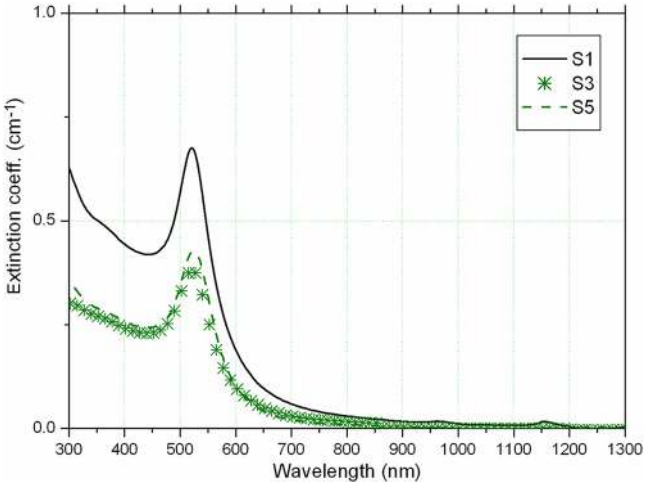

Fig. 7 Extinction coefficient of NPs decoupled from the base fluid contribution.

extinction coefficient of as-produced samples, obtained by means of the Lambert–Beer law from the experimental transmittance corrected for the reflectance term. Again, the surface plasmonic peak (transverse surface plasmon resonance) can be clearly recognized, as well as a secondary small shoulder at wavelengths below 400 nm, in agreement with the literature.[45]

The small features at around 965 and 1157 nm are probably due to instrumental artifacts, as the contingent presence of nonspherical particles exhibiting longitudinal surface plasmon resonances in this spectral region[46] could be ruled out by TEM analyses. The difference in the absolute value of the extinction coefficient for the different samples can be ascribed to the different particle size distribution and polydispersion, and distribution of NPs concentration, as mentioned above. The extinction coefficient $\mu_{\text{ext}}(\lambda)$ is the sum of the absorption and scattering coefficients. Thus, to give an estimation of the absorption properties of the nanofluid, it is also necessary to evaluate the light scattering characteristics. The spectral scattering albedo $\omega(\lambda)$ is defined as the ratio between scattering and extinction coefficients and can be obtained from the calculated extinction and scattering efficiencies Q_{ext} and Q_{sca}, respectively. Following the notation in Ref. 47 they are given by

$$Q_{\text{ext}} = 4x\,\text{Im}\left\{\frac{m^2-1}{m^2+2}\left[1+\frac{x^2}{15}\left(\frac{m^2-1}{m^2+2}\right)\frac{m^4+27\,m^2+38}{2\,m^2+3}\right]\right\}+\frac{8}{3}x^4\,\text{Re}\left\{\left(\frac{m^2-1}{m^2+2}\right)^2\right\} \quad (1)$$

$$Q_{\text{sca}} = \frac{8}{3}x^4\left|\frac{m^2-1}{m^2+2}\right|^2, \tag{2}$$

where m is the complex relative refractive index

$$m = \frac{n_p + ik_p}{n_f + ik_f} \tag{3}$$

defined in terms of the real (n_p, n_f) and imaginary parts (k_p, k_f) of the complex refractive indexes of particles and fluid, respectively; and x is the particle size parameter

$$x = \frac{2\pi n_f \alpha}{\lambda}, \tag{4}$$

where α is the particle radius and λ the light wavelength in a vacuum. In the Rayleigh regime $|m|x \ll 1$, the expression in brackets in Eq. (1) is approximately unity. The extinction efficiency thus becomes

$$Q_{ext} = 4x\,\text{Im}\left\{\frac{m^2-1}{m^2+2}\right\} + \frac{8}{3}x^4\,\text{Re}\left\{\left(\frac{m^2-1}{m^2+2}\right)^2\right\}. \tag{5}$$

For polydispersed particles, the scattering albedo is given by[46]

$$\omega = \frac{\sum_i N_i Q_{\text{sca},i} \cdot \pi a_i^2}{\sum_i N_i Q_{\text{ext},i} \cdot \pi a_i^2}, \tag{6}$$

where N_i, $Q_{\text{sca},i}$, and $Q_{\text{ext},i}$ are the volume concentration, the scattering efficiency, and the extinction efficiency, respectively, of the spheres of radius a_i. Equation (6) was used to calculate the single-scattering albedo for our samples in the Rayleigh regime. The real and imaginary parts of the complex refractive index of water and gold considered in the calculation were taken from Refs. 48–50, considering spectral values in the range of wavelengths from 300 to 2300 nm. For the sake of simplicity, the experimental NPs size distributions (Fig. 4) have been approximated as trimodal dispersions, by considering, for each sample, the measured populations for three particle sizes around the peak of the distribution and including at least 85% of the total number of particles. It should be noticed that the Rayleigh hypothesis is not satisfied for wavelengths in the range around 300 to 350 nm for the largest particles in the distribution (which represent about 30%, 20%, and 5% of the population considered in samples S1, S5, and S3, respectively). Thus, in this spectral region, the scattering albedo is probably underestimated. The spectral scattering albedo $\omega(\lambda)$ was used to obtain the spectral absorption coefficient $\mu_{\text{abs}}(\lambda)$ of the nanofluid from the experimental extinction coefficient $\mu_{\text{ext}}(\lambda)$ as

$$\mu_{\text{abs}}(\lambda) = \mu_{\text{ext}}(\lambda)[1 - \omega(\lambda)]. \tag{7}$$

To quantitatively evaluate the sunlight absorption capability of samples for the proposed solar collector application, calculations were performed to determine the fraction F of the incident power absorbed in the fluid after a path length l within it

$$F(\lambda) = 1 - \frac{\int_{\lambda_{\text{min}}}^{\lambda_{\text{MAX}}} I(\lambda) \cdot e^{-\mu_{\text{abs}}(\lambda)l}\text{d}\lambda}{\int_{\lambda_{\text{min}}}^{\lambda_{\text{MAX}}} I(\lambda)\text{d}\lambda}, \tag{8}$$

where $I(\lambda)$ is the spectral distribution of the incident irradiance integrated in the wavelength range $(\lambda_{\text{min}}, \lambda_{\text{MAX}})$. For a still and cold isotropic medium, $\mu_{\text{abs}}(\lambda)$ is considered constant along l. In Fig. 8, the calculated absorbed light fraction is compared as a function of the propagation depth within the fluid for pure water and for the as-produced gold nanofluids. The calculation has been performed according to Eq. (8), keeping the CIE solar spectrum with air mass $m = 1.5$[51] as $I(\lambda)$ and considering $\lambda_{\text{min}} = 300$ nm and $\lambda_{\text{MAX}} = 2300$ nm.

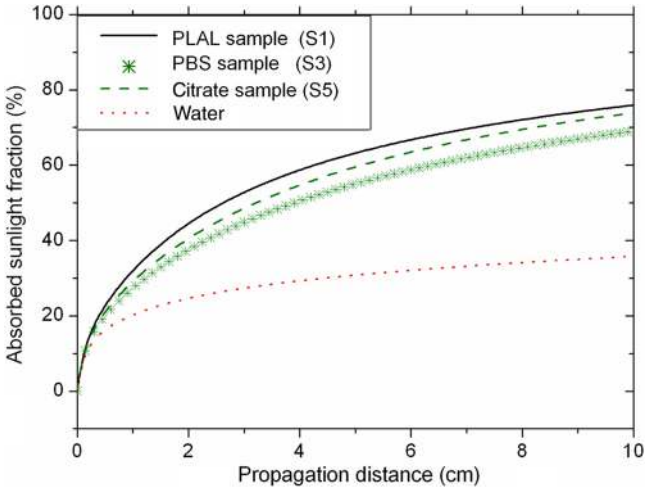

Fig. 8 Absorbed sunlight fraction as a function of the propagation distance in the nanofluid for the as-produced samples.

It can be observed that even with the low concentrations considered, an absorption of nearly 80% can be obtained after a 10-cm propagation length in the nanofluid. This value is nearly twice that obtained for simple water. The samples show small absorption differences due to the differences in their extinction coefficient mentioned above. A larger absorption can be obtained with more concentrated suspensions. The results shown demonstrate that gold NP-based nanofluids can be used as volume absorbers in direct absorption solar collectors. Moreover, they also offer the opportunity to optimize the sunlight absorption for the specific solar collector architecture of interest by changing the concentration and sizes of NPs.

3.3 *Thermal Properties*

As noted before, one of the first applications of nanofluids was their use as heat transfer fluids due to their improved thermal properties, thermal conductivity being one of the key properties. In this work, the thermal conductivity of nanofluids produced by PLAL-PF and commercial nanofluids was measured at 80°C. Six measurements were performed for each sample. The experimental error could be determined at a confidence level of 95%. Results are shown in Table 3. It can be observed that the thermal conductivity of the base fluid always increases when NPs are present, as expected. Differences between PLAL-PF and commercial nanofluids, as well as before and after cycling, lie within the experimental uncertainty. Therefore, it can be concluded that PLAL-PF nanofluids provide an increase in thermal conductivity similar to commercial suspensions and stable with thermal cycling. As a final comment, it should be noted that the nanofluids investigated have a very low particle concentration. A larger thermal conductivity enhancement can be obtained with more concentrated suspensions.[52] However, as the NPs concentration increases, nanofluids could show stability problems, which, in the case of chemically

Table 3 Thermal conductivity measurements at 80°C.

	k (W/m · K)		Δk (%)	
Sample	Not cycled	Cycled	Not cycled	Cycled
Distilled water	0.652 ± 0.013	—	—	—
PLAL-PF	0.667 ± 0.018	0.666 ± 0.020	2.23	2.20
Commercial PBS	0.687 ± 0.022	0.677 ± 0.010	5.42	3.88
Commercial citrate	0.681 ± 0.009	0.669 ± 0.013	4.36	2.53

stabilized samples, translates into the need for a higher amount of surfactant with a detrimental effect on the thermal conductivity properties themselves.[53] Within this framework, physical techniques like PLAL-PF, which are able to produce stable nanofluids without the use of surfactants, can have an even larger impact.

4 Conclusion

This work reports on the production, by means of the PLAL-PF technique without the use of chemical additives, of gold NP-based aqueous nanofluids. The laser-produced samples have been compared with PBS and citrate chemically stabilized commercial suspensions as regards to their composition, NP's shape and size distribution, optical properties, thermal transfer coefficient, and stability under thermal cycling. While offering the great advantage of a higher purity with no need for additional chemicals, PLAL-PF samples show physical properties comparable to commercial chemically stabilized samples and in some cases even better for their potential use in the harvesting of energy industry, e.g., a higher sphericity of suspended particles, which could lead to a better nanofluid motion or the purity of the particles. In all cases, nanofluids have been shown to be able to work in thermal cycling. The stability of PLAL-PF samples under cycling appears to be better than that of citrate samples and comparable to that of PBS-stabilized nanofluids. From the measured extinction coefficient and the calculated spectral scattering albedo, sunlight absorption characteristics have been assessed with a view to the possible use of gold-NP nanofluids as direct absorbers in solar collectors. It should be noted that optical absorption can be tuned by changing the concentration and size of the NPs. Moreover, it is known that the thermal conductivity of nanofluids increases with the NP volume load. Thus, the advantage of using the PLAL-PF technique, which produces stable nanofluids without chemical surfactants, can be even larger when high NP concentrations are required.

Acknowledgments

This work was partially funded by the Generalitat Valenciana through the programme PROMETEO–2012–021, and by the Universitat Jaume I through the projects P1·1B2013–43 and P1·1B2013–53. Financial support from the Spanish Ministry of Science FIS2013–40666–P is also acknowledged. The authors are also very grateful to the Servicios Centrales de Instrumentación Científica (SCIC) of the Universitat Jaume I for the use of the femtosecond laser. R. Torres-Mendieta gratefully acknowledges the Generalitat Valenciana support from the Santiago Grisolia scholarship GRISOLIA/2013/015. The Italian bank foundation "Fondazione Ente Cassa di Risparmio di Firenze" is gratefully acknowledged for providing the grant for M. Meucci within the framework of the "SOLE" and "SOLE-2" projects (pratiche n. 2013.0726 and 2014.0711). Thanks are due to Mr. Mauro Pucci and Mr. Massimo D'Uva from CNR-INO for technical assistance.

References

1. D. Wen et al., "Review of nanofluids for heat transfer applications," *Particuology* **7**, 141–150 (2013).
2. J. C. Maxwell, *A Treatise on Electricity and Magnetism*, Clarendon Press, Oxford, United Kingdom (1873).
3. S. U. S. Choi, "Enhancing thermal conductivity of fluids with nanoparticles," in *Proc. of the ASME Int. Mechanical Engineering Congress and Exposition*, FED 231/MD, 66, pp. 99–105, ASME, San Francisco, California (1995).
4. S. K. Das et al., *Nanofluids Science and Technology*, John Wiley and Sons Inc., Hoboken, New Jersey (2008).
5. R. S. Vajjha and D. K. Das, "A review and analysis on influence of temperature and concentration of nanofluids on thermophysical properties, heat transfer and pumping power," *Int. J. Heat Mass Transfer* **55**, 4063–4078 (2012).

6. W. Yu et al., "Comparative review of turbulent heat transfer of nanofluids," *Int. J. Heat Mass Transfer* **55**, 5380–5396 (2012).
7. B. H. Salman et al., "Characteristics of heat transfer and fluid flow in microtube and microchannel using conventional fluids and nanofluids: a review," *Renewable Sustainable Energy Rev.* **28**, 848–880 (2013).
8. A. M. Hussein et al., "A review of forced convection heat transfer enhancement and hydrodynamic characteristics of a nanofluid," *Renewable Sustainable Energy Rev.* **29**, 734–743 (2014).
9. J. A. Eastman et al., "Anomalously increased effective thermal conductivities of ethylene glycol-based nanofluids containing copper nanoparticles," *Appl. Phys. Lett.* **78**, 718–720 (2001).
10. L. Godson et al., "Experimental investigation on the thermal conductivity and viscosity of silver-deionized water nanofluid," *Exp. Heat Transfer* **23**, 317–332 (2010).
11. S. W. Lee et al., "Investigation of viscosity and thermal conductivity of SiC nanofluids for heat transfer applications," *Int. J. Heat Mass. Transfer* **54**, 433–438 (2011).
12. H. Xie et al., "Thermal conductivity enhancement of suspensions containing nanosized alumina particles," *J. Appl. Phys.* **91**, 4568–4572 (2002).
13. S. U. S. Choi et al., "Anomalous thermal conductivity enhancement in nanotube suspensions," *App. Phys. Lett.* **79**, 2252 (2001).
14. E. Sani et al., "Carbon nanohorns-based nanofluids as direct sunlight absorbers," *Opt. Express* **18**, 5179–5187 (2010).
15. L. Chen, W. Yu, and H. Xie, "Enhanced thermal conductivity of nanofluids containing Ag/MWNT composites," *Powder Technol.* **231**, 18–20 (2012).
16. J. E. Minardi and H. N. Chuang, "Performance of black liquid flat-plate solar collector," *Solar Energy* **17**, 179–183 (1975).
17. T. P. Otanicar et al., "Nanofluid-based direct absorption solar collector," *J. Renewable Sustainable Energy* **2**, 033102 (2010).
18. A. Moradi et al., "Carbon-nanohorn based nanofluids for a direct absorption solar collector for civil application," *J. Nanosci. Nanotech.* **15**, 3488–3495 (2015).
19. A. Lenert and E. N. Wang, "Optimization of nanofluid volumetric receivers for solar thermal energy conversion," *Solar Energy* **86**, 253–265 (2012).
20. Z. Luo et al., "Performance improvement of a nanofluid solar collector based on direct absorption collection (DAC) concepts," *Int. J. Heat Mass Transfer* **75**, 262–271 (2014).
21. R. Saidur et al., "Evaluation of the effect of nanofluid-based absorbers on direct solar collector," *Int. J. Heat Mass Transfer* **55**, 5899–5907 (2012).
22. Y. Kameya and K. Hanamura, "Enhancement of solar radiation absorption using nanoparticle suspension," *Solar Energy* **85**, 299–307 (2011).
23. E. Sani et al., "Potential of carbon nanohorn-based suspensions for solar thermal collectors," *Solar Energy Mater. Solar Cells* **95**, 2994–3000 (2011).
24. E. Sani et al., "Optical properties of mixed nanofluids containing carbon nanohorns and silver nanoparticles for solar energy applications," *J. Nanosci. Nanotech.* **15**, 3568–3573 (2015).
25. R. A. Taylor et al., "Nanofluid optical property characterization: towards efficient direct absorption solar collectors," *Nanoscale Res. Lett.* **6**, 225 (2011).
26. R. Prasher, P. E. Phelan, and P. Bhattacharya, "Effect of aggregation kinetics on the thermal conductivity of nanoscale colloidal solutions (nanofluid)," *Nano Lett.* **6**, 1529–1534 (2006).
27. J. W. Gao et al., "Experimental investigation of heat conduction mechanisms in nanofluids. Clue on clustering," *Nano Lett.* **9**, 4128–4132 (2009).
28. P. P. Patil et al., "Pulsed-laser induced reactive quenching at liquid-solid interface: aqueous oxidation of iron," *Phys. Rev. Lett.* **58**, 238–241 (1987).
29. A. Pyatenko et al., "Mechanism of pulse laser interaction with colloidal nanoparticles," *Laser Photonics Rev.* **7**, 596–604 (2013).
30. R. Streubel, S. Barcikowski, and B. Gökce, "Continuous multigram nanoparticle synthesis by high-power, high-repetition-rate ultrafast laser ablation in liquids," *Opt. Lett.* **41**, 1486 (2016).

31. S. Besner, A. V. Kabashin, and M. Meunier, "Two-step femtosecond laser ablation-based method for the synthesis of stable and ultra-pure gold nanoparticles in water," *Appl. Phys. A.* **88**, 269–272 (2007).
32. F. A. Videla et al., "Analysis of the main optical mechanisms responsible for fragmentation of gold nanoparticles by femtosecond laser radiation," *J. Appl. Phys.* **107**, 114308 (2010).
33. R. Torres-Mendieta et al., "Fabrication of gold nanoparticles in Therminol VP-1 by laser ablation and fragmentation with fs pulses," *Laser Phys. Lett.* **11**, 126001 (2014).
34. A. V. Kabashin and M. Meunier, "Synthesis of colloidal nanoparticles during femtosecond laser ablation of gold in water," *J. Appl. Phys.* **94**, 7941–7943 (2003).
35. A. H. Chin, R. W. Schonlein, and T. E. Glover, "Ultrafast structural dynamics in InSb probed by time-resolved x-ray diffraction," *Phys. Rev. Lett.* **83**, 336–339 (1999).
36. J. Sylvestre et al., "Stabilization and size control of gold nanoparticles during laser ablation in aqueous cyclodextrins," *J. Am. Chem. Soc.* **126**, 7176–7177 (2004).
37. H. Muto et al., "Estimation of surface oxide on surfactant-free gold nanoparticles laser-ablated in water," *J. Phys. Chem. C*, **111**, 17221–17226 (2007).
38. A. Hahn, S. Barcikowski, and B. N. Chichkov, "Influences on nanoparticle production during pulsed laser ablation," *J. Laser Micro/Nanoeng.* **3**, 73–77 (2008).
39. F. Hajiesmaeilbaigi et al., "Preparation of silver nanoparticles by laser ablation and fragmentation in pure water," *Laser Phys. Lett.* **3**, 252–256 (2006).
40. A. Menendez-Manjon, P. Wagener, and S. Barcikowski, "Transfer-matrix method for efficient ablation by pulsed laser ablation and nanoparticle generation in liquids," *J. Phys. Chem. C.* **115**, 5108–5114 (2011).
41. S. Link and M. El-Sayed, "Shape and size dependence of radiative, non-radiative and photothermal properties of gold nanocrystals," *Int. Rev. Phys. Chem.* **19**, 409–453 (1999).
42. P. H. D. Ferreira et al., "Femtosecond laser induced synthesis of Au nanoparticles mediated by chitosan," *Opt. Express* **20**, 518–523 (2012).
43. B. Tangeysh et al., "Gold nanoparticle synthesis using spatially and temporally shaped femtosecond laser pulses: post-irradiation auto-reduction of aqueous [AuCl4]," *J. Phys. Chem. C.* **117**, 18719–18727 (2013).
44. X. Liu et al., "Extinction coefficient of gold nanoparticles with different sizes and different capping ligands," *Colloids Surf. B* **58**, 3–7 (2007).
45. S. Boopathi, S. Senthilkumar, and K. L. Phaniet, "Facile and one pot synthesis of gold nanoparticles using tetraphenylborate and polyvinylpyrrolidone for selective colorimetric detection of mercury ions in aqueous medium," *J. Anal. Method Chem.* **348965**, 6 (2012).
46. C. F. Bohren and D. R. Huffman, *Absorption and Scattering of Light by Small Particles*, Wiley, Hoboken, New Jersey (1983).
47. S. J. Madsen, M. S. Patterson, and B. C. Wilson, "The use of India ink as an optical absorber in tissue-simulating phantoms," *Phys. Med. Biol.* **37**, 985–993 (1992).
48. G. M. Hale and M. R. Querry, "Optical constants of water in the 200 nm to 200 μm wavelength," *Reg. Appl. Opt.* **12**, 555–563 (1973).
49. A. D. Rakic et al., "Optical properties of metallic films for vertical-cavity optoelectronic devices," *Appl. Opt.* **37**, 5271–5283 (1998).
50. Numerical values of complex refractive index of Au, calculated from the parameters reported in Ref. 48 are available on the refractiveindex.info database: http://refractiveindex.info/?shelf=main&book=Au&page=Rakic from Ref. 49.
51. CIE Technical Report no. 85, "Solar Spectral Irradiance," (Technical Report, 1989).
52. V. Trisaksri and S. Wongwises, "Critical review of heat transfer characteristics of nanofluids," *Renewable Sustainable Energy Rev.* **11**, 512–523 (2007).
53. Z. Mingzheng et al., "Analysis of factors influencing thermal conductivity and viscosity in different kinds of surfactant solutions," *Exp. Therm. Fluid Sci.* **36**, 22–29 (2012).

Biographies for the authors are not available.